Electronic Supplementary Material (ESI) for CrystEngComm.

Supporting Information for:

Understanding the structural landscape of Mn-based MOFs formed with hinged pyrazole carboxylate linkers

Josephine F. Smernik,[a] Pol. Gimeno-Fonquernie,[a] Jorge Albalad,[a] Tyla S. Jones,[a] Rosemary J. Young,[a,b] Neil R. Champness,[b,c] Christian J. Doonan,[a] Jack D. Evans[a] and Christopher J. Sumby[a*]

[a.] *Department of Chemistry and the Centre for Advanced Nanomaterials, The University of Adelaide, Adelaide, SA 5005, Australia. Email: christopher.sumby@adelaide.edu.au*
[b.] *School of Chemistry, The University of Nottingham, Nottingham, UK.*
[c.] *School of Chemistry, The University of Birmingham, Birmingham, UK.*

Table of Contents

S1. Additional Synthetic Procedures

S1.1. H_2L1^{Me}

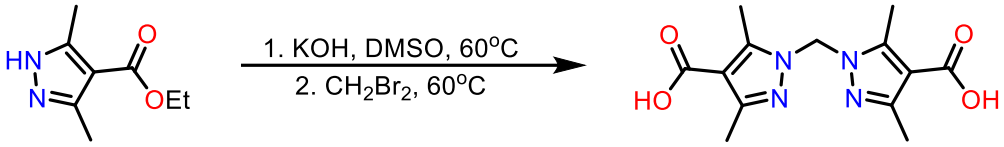

1,1-Methylenebis(3,5-dimethyl-1H-pyrazole-4-carboxylic acid) (H_2L1^{Me}): Ethyl-3,5-dimethyl-1H-pyrazole-4-carboxylate was synthesized as previously reported.[1] Ethyl-3,5-dimethyl-1H-pyrazole-4-carboxylate (4.3 g, 25.7 mmol) and freshly powdered potassium hydroxide (8.25 g, 147 mmol) were dissolved in DMSO (30 mL) and the solution was stirred at 60°C for 1h. A solution of dibromomethane (0.868 mL, 12.7 mmol) in DMSO (10 mL) was added dropwise to the stirring solution and it was stirred at 60°C overnight. The solution was poured into distilled water (200 mL) and washed with chloroform (5 × 30 mL). The aqueous phase was acidified to pH3 with HCl to precipitate H_2L1^{Me} as a while solid. The solid was filtered, washed with water, ethanol, diethyl ether and dried under reduced pressure to give H_2**L1^{Me}** (2.9 g, 78 %). IR (cm^{-1}): 1653, 1553, 1436, 1373, 1316, 1249,1165; ^{1}H NMR (500 MHz, DMSO-d6) δ 12.27 (br, s, 2H), 6.21 (s, 2H), 2.65 (s, 6H), 2.23 (s, 6H).

S1.2. H_4L5

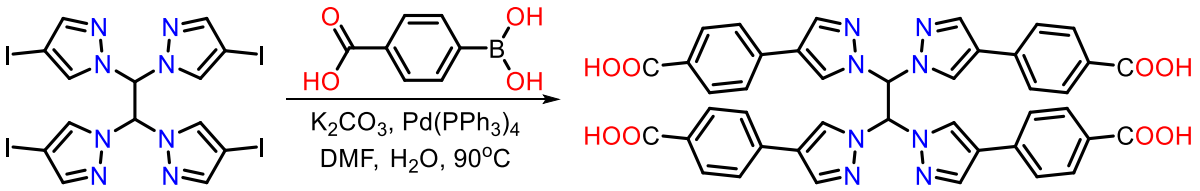

1,1,2,2-Tetrakis[4-(4-carboxyphenyl)-1H-pyrazol-1-yl]ethane (H_4L5): 1,1,2,2-tetrakis(4-iodo-1H-pyrazol-1-yl)ethane was synthesised as previously reported.[2] A mixture of DMF (90 mL) and water (20 mL) was stirred and degassed under Ar at 25°C for 30 mins. Then, a dry mixture containing 1,1,2,2-tetrakis(4-iodo-1H-pyrazol-1-yl)ethane (1.5 g, 1.9 mmol), 4-carboxylphenyl boronic acid (1.8 g, 10.8 mmol), K_2CO_3 (6.82 g, 49 mmol) and $Pd(PPh_3)_4$ (180 mg, 0.16 mmol) was added to the stirring solution. The mixture was then degassed and heated at 90°C for 3 days. The mixture was added to water (300 mL), filtered using celite, and washed with $CHCl_3$ (2 × 50 mL). The remaining solution was acidified to pH3 using 2M HCl to produce a white precipitate. This was separated by centrifugation, washed with water and 30% ethanol in water, and dried under vacuum to give H_4**L5** as a white powder. Yield: 0.7 g (47%). IR (cm^{-1}): 1701, 1611, 1565, 1415, 1226, 1178; ^{1}H NMR (500 MHz, DMSO-d_6): 12.86 (br s, 4H, COOH), 8.82 (s, 4H, pyrH), 8.42 (s, 2H, N-CHR-N), 8.07 (s, 4H, pyrH), 7.88 (d, 10 Hz, 8H, ArH), 7.62 (d, 10 Hz, 8H, ArH).

S2. Supporting single crystal X-ray diffraction (SCXRD) structures

S2.1. MnMOF-L2 ([Mn(L2)(H_2O)$_2$])

MnMOF-L2 has a 2D layered structure similar to MnMOF-2D. It features linear Mn chains where each Mn(II) ion is connected to four carboxylates in a square planar geometry with two capping water molecules, leading to an overall octahedral geometry (Figure S1d). The Mn chains are linked by ligands to form 2D layers (Figure S1a), which stack on top of each other, with the Mn chains of one layer sitting on top of the bispyrazole units of the next layer (Figure S1b). The ligand is fully coordinated through the carboxylate sites but the bispyrazole is uncoordinated and in the syn-conformation (Figure S1c).

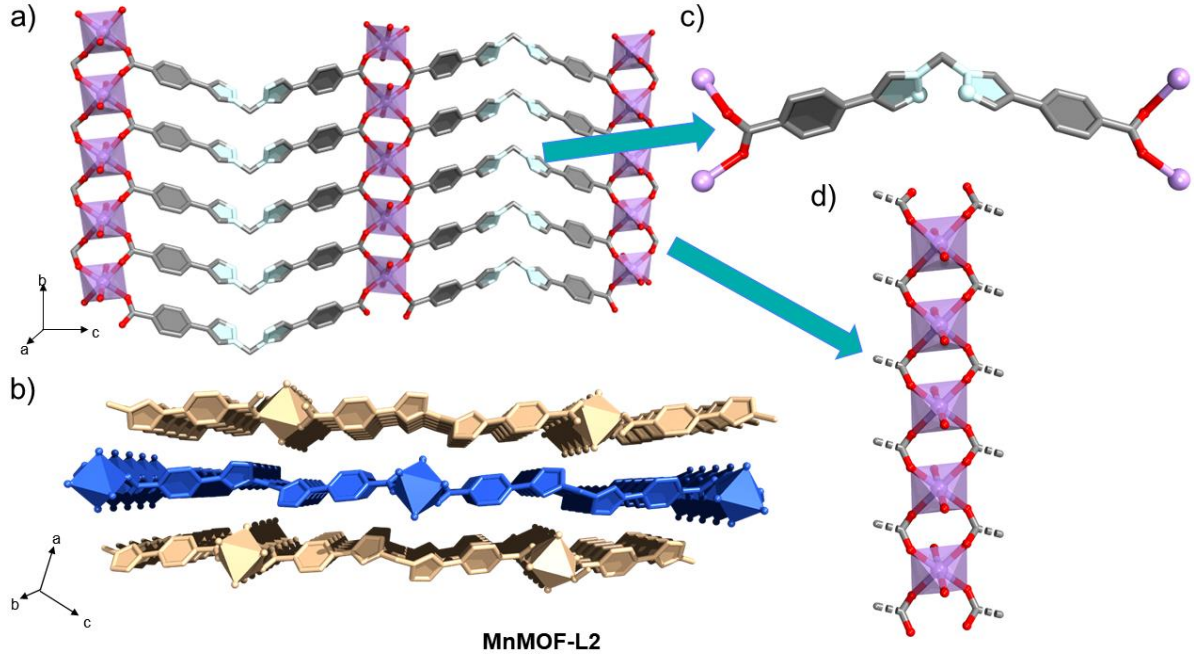

Figure S1. Additional structural details for MnMOF-L2. a) A representation of a single layer of MnMOF-L2 in the *bc* plane. b) A side on view of the layer packing of MnMOF-L2. c) A ligand of MnMOF-L2 showing coordination through each carboxylate oxygen atom and an uncoordinated bispyrazole unit. d) A view of a Mn chain in the structure, which consists of each Mn(II) ion being coordinated through 4 carboxylates to 2 other Mn(II) ions. (C, grey; N, light blue; O, red; Mn, purple). Hydrogens have been omitted for clarity.

S2.2. MnMOF-L1^{Me} ([Mn_2(L1^{Me})$_2$(H_2O)$_4$])

MnMOF-L1^{Me} crystallised in the monoclinic space group $P2_1/c$ with an asymmetric unit that contains two Mn atoms, two ligands and four water molecules. The Mn atoms are each bound by 6 oxygen atoms in a canted octahedral geometry and arranged in pillars extending along the *a* axis (Figure S2a). Alternating gaps between Mn atoms in the pillars are bridged by carboxylate groups from three **L1^{Me}** ligands or by one bridging ligand with the other two sites on each Mn centre occupied by *cis*-coordinated water molecules. All ligand molecules are coordinated through all carboxylate oxygens, allowing them to bridge along the Mn pillars and between pillars (Figure S2b). The ligands protrude from these pillars to connect each pillar to four others in the *bc* plane. All bispyrazole groups, which are non-coordinated, adopt the anti-conformation. The overall packing is further stabilised by intra-pillar and inter-pillar hydrogen bonding interactions by the coordinated water molecules to give a close packed structure (Figure S2c/S2d).

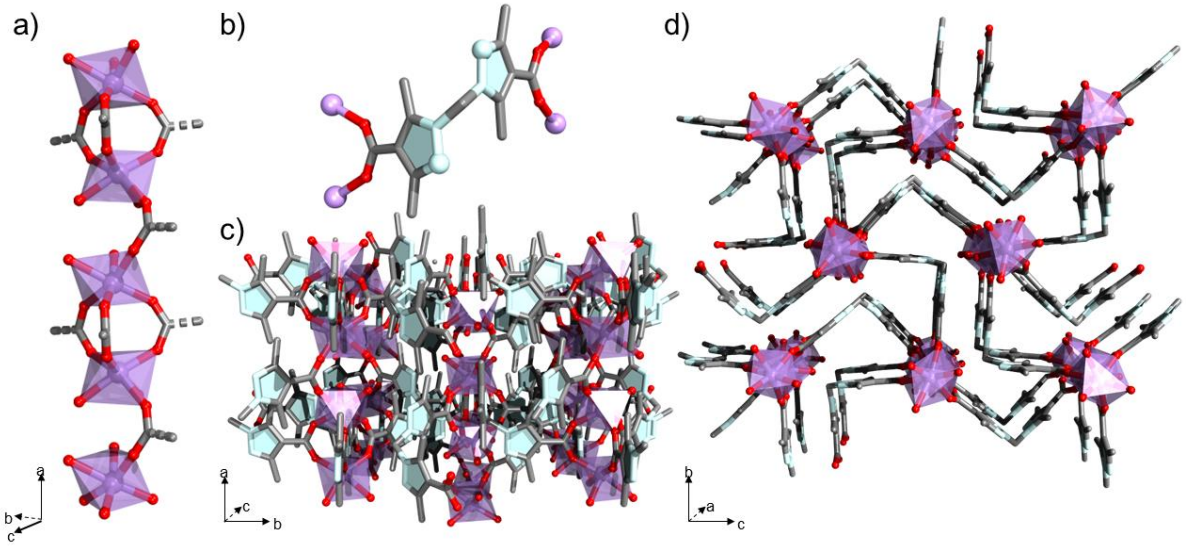

Figure S1. Additional structural details for MnMOF-L1^{Me}. a) A view of a Mn chain in the structure, which consists of a Mn dimer bridged by three carboxylates that is in turn connected to the next dimer by a single bridging carboxylate. b) A view of the ligand with coordinated carboxylates and bispyrazole units in the anti position. c) and d) Representations of MnMOF-L1^{Me} viewed down the c) *c* axis and d) *a* axis showing the Mn chains and the densely packed, non-coordinated pyrazole groups. (C, grey; N, light blue; O, red; Mn, purple). Hydrogens have been omitted for clarity.

S2.3. MnMOF-L1-1 ([Mn_2**L1**$_2(H_2O)_3$]·$2H_2O$)

The structure of MnMOF-L1-1 ([Mn_2**L1**$_2(H_2O)_3$]·$2H_2O$) is a 3D coordination polymer comprising individual Mn(II) atoms that are coordinated by the bis-pyrazole unit of one ligand, a monodentate carboxylate donor from two additional ligands and two water molecules in the axial coordination sites. This coordination environment has been commonly encountered for related ligands (e.g. **L2** and **L2^{Me}**) and 3d transition metals (e.g. Cu(II), Co(II) and Ni(II))[3, 4]. Like the previously reported Cu structure, the axial water molecules form hydrogen bonds to adjacent carboxylate oxygen atoms from the linkers. The overall 3D structure can be rationalised by considering each Mn centre as a four-connecting node. Within the layers of Mn atoms in the *ab* plane each Mn centre is connected through carboxylates to two linkers where the pyrazole groups point in opposite directions and through a bispyrazole group to a third linker (Figure S3c). The differences in height of Mn centres in the *c* direction leads to the overall 3D structure (Figure S3d/S3e). In addition, each Mn centre is located above and below other Mn centres where the pyrazole chelate rings point opposite, allowing for hydrogen bonding (Figure S3a). Each ligand is coordinated to Mn atoms through its bispyrazole unit and one carboxylate oxygen on each side (Figure S3b). MnMOF-L1-1 adopts a needle-like crystal habit and the compound crystallises in the monoclinic space group *Cc* with a full ligand, a Mn centre and two coordinated water molecules in the asymmetric unit. The linker and Mn centre are disordered over two positions with each position relating to a different 3D coordination polymer with opposite handedness (ratio of 0.64:0.36 by refinement).

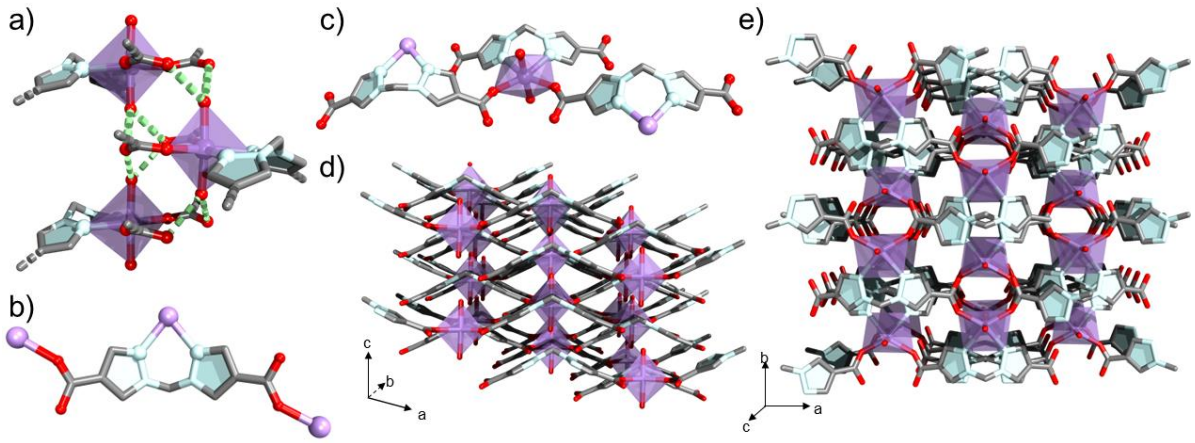

Figure S3. Additional structural details for MnMOF-L1-1 a) Three Mn centres connected through hydrogen bonding to form a pillar in the *c* direction. b) A single ligand of MnMOF-L1-1 which coordinates through the bispyrazole unit and one carboxylate oxygen on each side. c) Ligands around a Mn centre. The two ligands coordinated through their carboxylates to the central Mn have bispyrazole units and corresponding coordinated Mn atoms facing opposite directions. d) Representation of MnMOF-L1-1 viewed side-on and looking down the *b*-axis with the hydrogen bonded Mn pillars visible in the *c* direction. e) Representation of MnMOF-L1-1 viewed from the *c* direction showing a top view of the Mn pillars and bispyrazole units of alternating orientation in the *b* direction. (C, grey; N, light blue; O, red; Mn, purple). Hydrogens have been omitted for clarity.

S2.4. MnMOF-L1-2 ($[Mn_2L1_2(H_2O)_3]\cdot 2H_2O$) and MnMOF-L1-3 ($[Mn_2\mathbf{L1}_2(H_2O)_2(DMF)]$)

The two additional phases encountered are both 2D materials; MnMOF-L1-2 ($[Mn_2L1_2(H_2O)_3]\cdot 2H_2O$) (Figure S4a-d) formed as a by-product during synthesis of the main phase when water adventitiously leaked from the vial during the heating process, and MnMOF-L1-3 ($[Mn_2\mathbf{L1}_2(H_2O)_2(DMF)]$) (Figure S4g-j) was formed by the use of less water initially. MnMOF-L1-2 forms as block shaped colourless crystals in the space group *Pnnm*, with an asymmetric unit that contains two distinct half ligand molecules, two half occupied Mn atoms on a mirror plane, three half occupied coordinated water molecules (one bridging and two terminal) and two half occupied water solvate molecules. MnMOF-L1-3 by comparison forms as rhombus-shaped crystals that crystallise in the triclinic space group *P*1 with an entire formula unit in the asymmetric unit. In MnMOF-L1-2, one Mn atom has an octahedral geometry with the equatorial sites occupied by carboxylate oxygens from four different ligands, and the axial sites occupied by a terminal water molecule and a bridging water molecule (Figure S4a) (in MnMOF-L1-3 the terminal water is replaced by DMF (Figure S4g)). The other Mn atom, which has an identical geometry in both materials, has a distorted octahedral geometry with two cis equatorial sites occupied by carboxylate oxygens from the two ligands which bridge the two Mn atoms, and the other equatorial sites occupied by a capping bispyrazole moiety. The coordination environment is completed by a terminal and the bridging water molecule. Of the two crystallographically distinct ligands, one is bound only through one carboxylate oxygen donor and has the bispyrazole group non-coordinated and in the syn conformation, yet the second is saturated and coordinated to five different Mn centres (Figure S4f).

Despite the very similar coordination environments, and overall structures, there are some interesting differences in the local conformation that affect the layered structures of phase 2 $[Mn_2\mathbf{L1}_2(H_2O)_3]\cdot 2H_2O$ and phase 3 $[Mn_2\mathbf{L1}_2(H_2O)_2(DMF)]$. MnMOF-L1-2 has the chelating moiety of L1 directed away from the Mn_2 cluster and consequently the clusters are located

more centrally within the layer. Both materials are close-packed with pi-pi bonding enabling stacking of the 2D layers (Figure S4e) but there is some variance in how this is achieved. In MnMOF-L1-3 the chelating bispyrazole directs the carboxylate donors closer to the Mn_2 cluster leading to the clusters being on the edge of the layer (Figure S4i/S4j). Additionally, for MnMOF-L1-3 the layers are more densely packed and there is less interdigitation of the layers; for MnMOF-L1-2 the layers are more open and there is more interdigitation (Figure S4c/S4d) to form a material that is slightly less densely packed (MnMOF-L1-2 density = 1.67 gcm^{-1} vs MnMOF-L1-3 density = 1.80 gcm^{-1}).

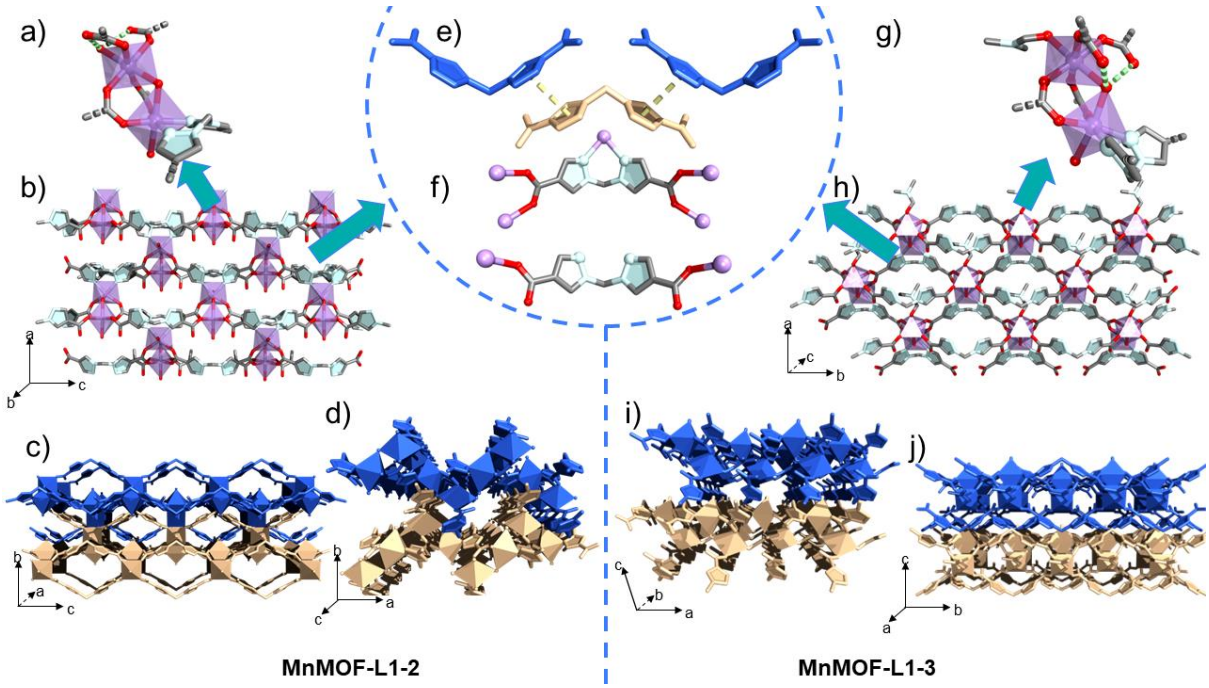

Figure S4. Additional structural details for MnMOF-L1-2 and MnMOF-L1-3. a) MnMOF-L1-2 Mn_2 cluster with water in the terminal position and the free carboxylates hydrogen bonding to this. b) A single layer MnMOF-L1-2 in the *ac* plane. c) Representation of the stacking of two layers of MnMOF-L1-2 in blue and yellow. Note that the two layers have significant interdigitation. d) Two layers of MnMOF-L1-2 in blue and yellow viewed from the *c* direction where the zigzag within a layer leading to this interdigitation is visible. e) Pi-pi stacking between pyrazole groups of adjacent layers which is present in both MnMOF-L1-2 and MnMOF-L1-3. f) Two distinct ligands which are present in both structures: one is fully saturated whereas the other only coordinates through half its oxygens and the bispyrazole is uncoordinated in the syn position. g) MnMOF-L1-3 Mn_2 cluster with DMF instead of water in the terminal position and the carboxylates facing the opposite direction compared to MnMOF-L1-2. h) A monolayer of MnMOF-L1-3. i) A view of MnMOF-L1-3 along the *b* axis showing minimal overlap between layers. j) A view of MnMOF-L1-3 along the *a* axis showing the stacking of 2D layers with the Mn centres located towards the top edge of the layers. (C, grey; N, light blue; O, red; Mn, purple). Hydrogens have been omitted for clarity.

S3. Powder X-Ray Diffraction Data

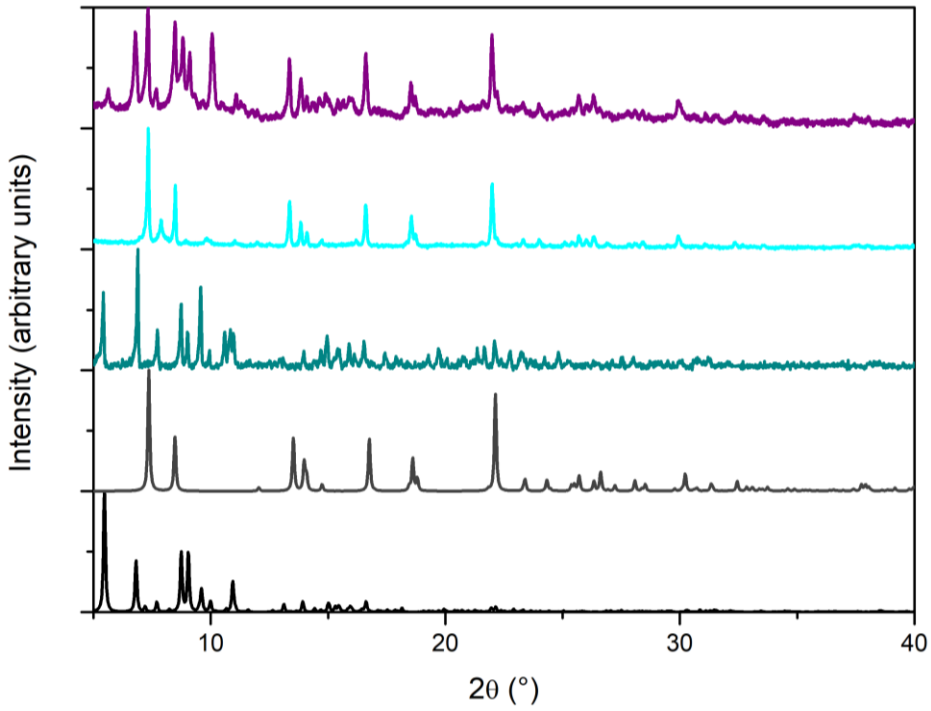

Figure S5. Experimental PXRD patterns for MnMOF-1 as made (teal), MnMOF-2D as made (aqua), and mixed-phase MnMOF-1 and MnMOF-2D (purple), plotted against simulated MnMOF-1 (black), and simulated MnMOF-2D (grey).

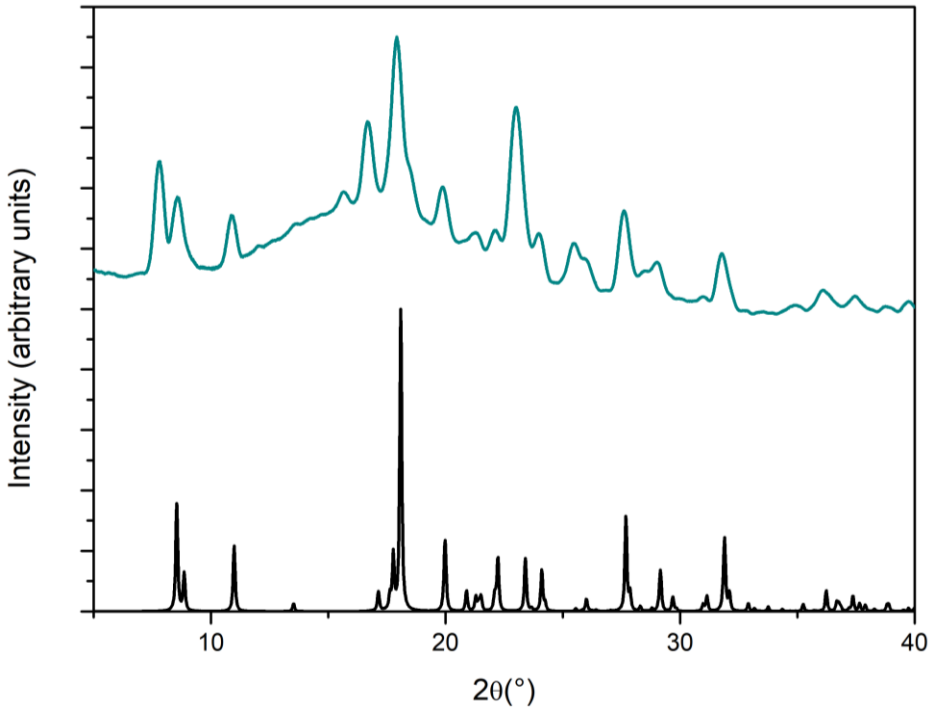

Figure S6. Experimental PXRD patterns for MnMOF-L2 as made (teal) plotted against simulated MnMOF-L2 (black). Due to the small amount of crystalline material formed, the experimental powder pattern was collected on an XtaLAB Synergy-S single crystal diffractometer in powder mode, which produces relatively broad peaks.

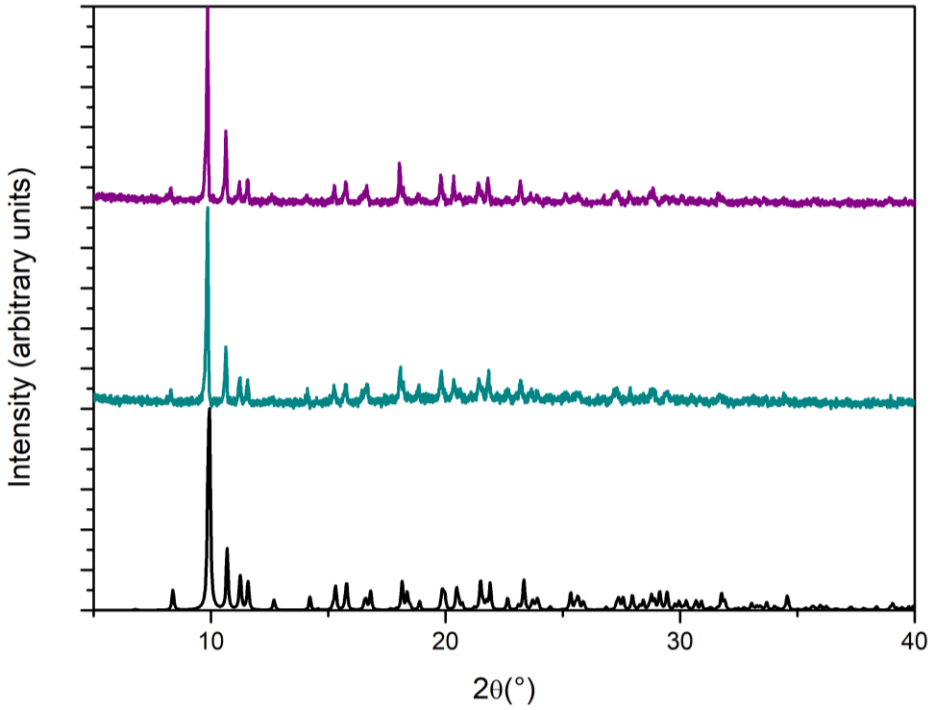

Figure S7. Experimental PXRD plots for MnMOF-L1^{Me} as made (teal), and MnMOF-L1^{Me} after drying (purple) plotted against simulated MnMOF-L1^{Me} (black).

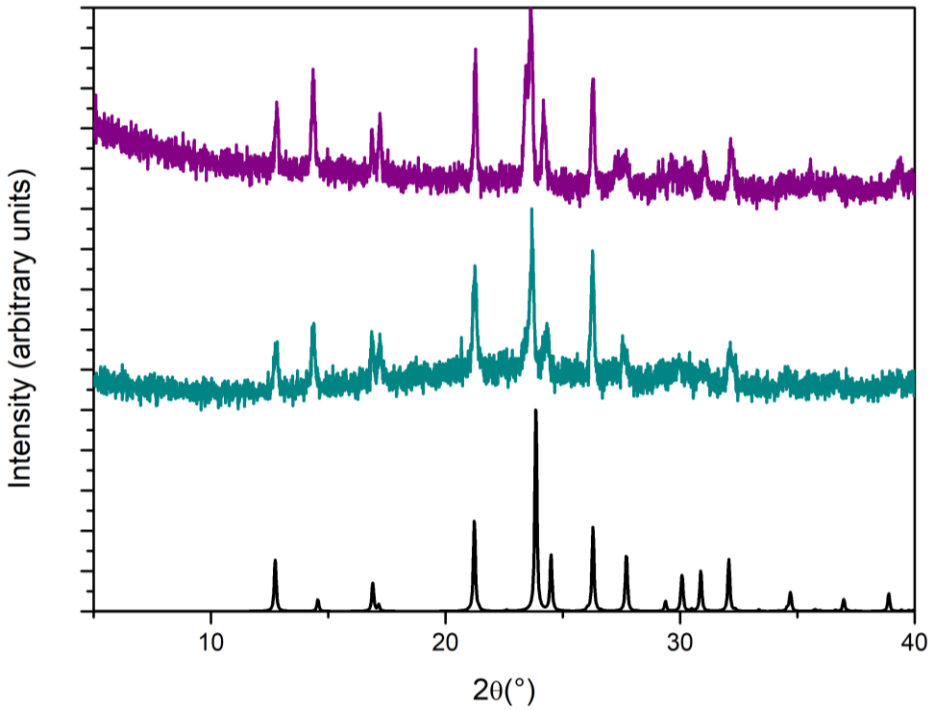

Figure S8. Experimental PXRD plots for MnMOF-L1-1 as made (teal), and MnMOF-L1-1 after drying (purple) plotted against simulated MnMOF-L1-1 (black).

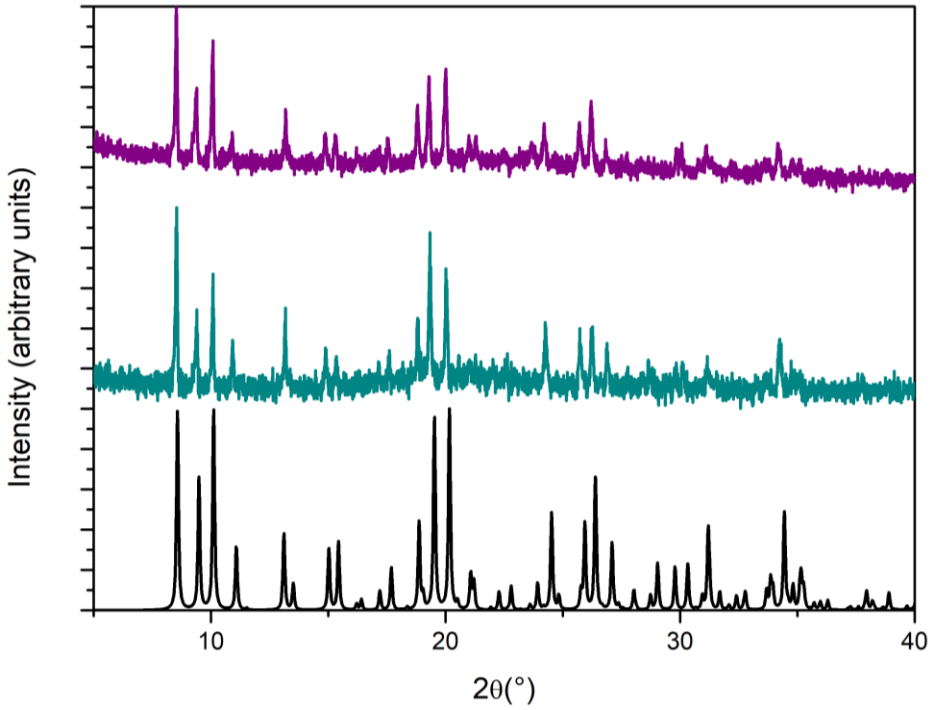

Figure S9. Experimental PXRD plots for MnMOF-L1-2 as made (teal), and MnMOF-L1-2 after drying (purple) plotted against simulated MnMOF-L1-2 (black).

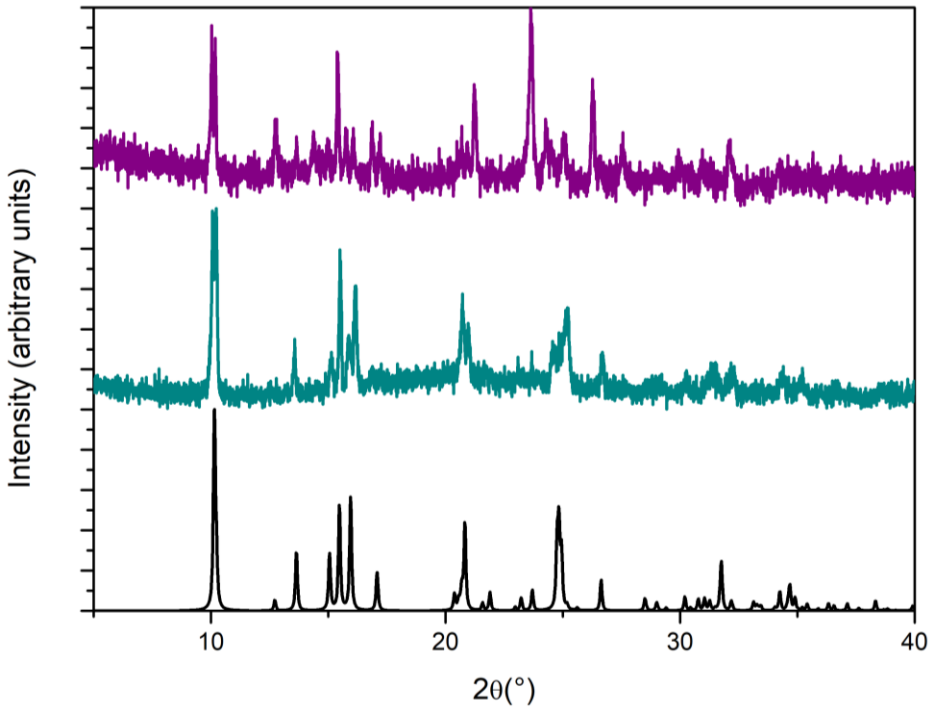

Figure S10. Experimental PXRD plots for MnMOF-L1-3 as made (teal), and MnMOF-L1-3 after drying (purple) plotted against simulated MnMOF-L1-3 (black).

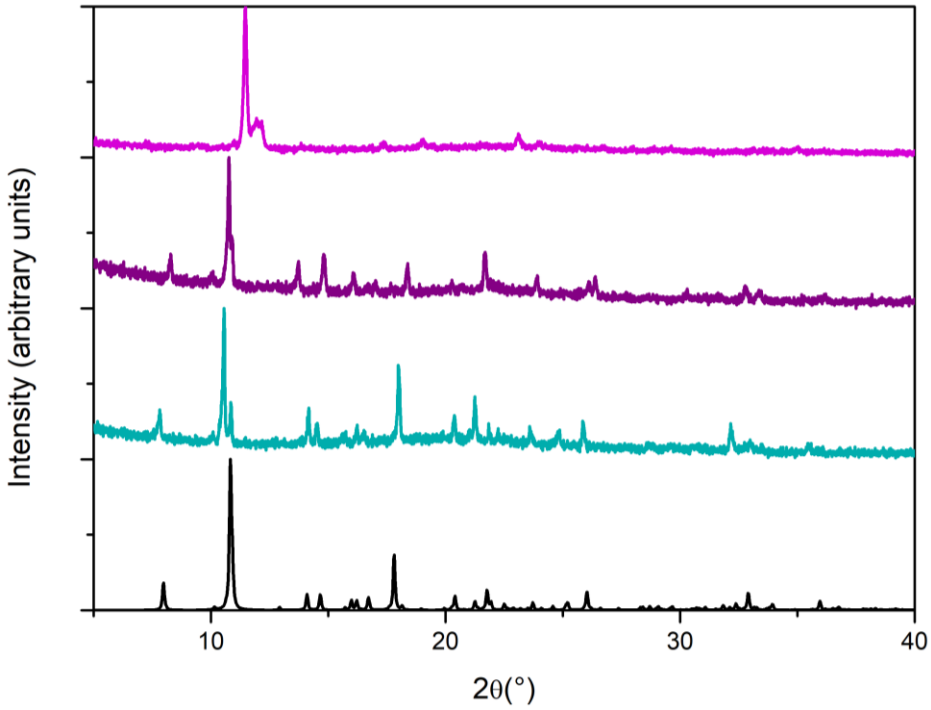

Figure S11. Experimental PXRD plots for MnMOF-L4 as made in DMF (teal), MnMOF-L4 in ethanol (purple), and MnMOF-L4 after adsorption (pink) plotted against simulated MnMOF-L4 (black). Like other flexible MOFs formed with these hinged links, the structure of dried MnMOF-L4 differs slightly from the solvated/as-synthesised material as the structures change upon desolvation.

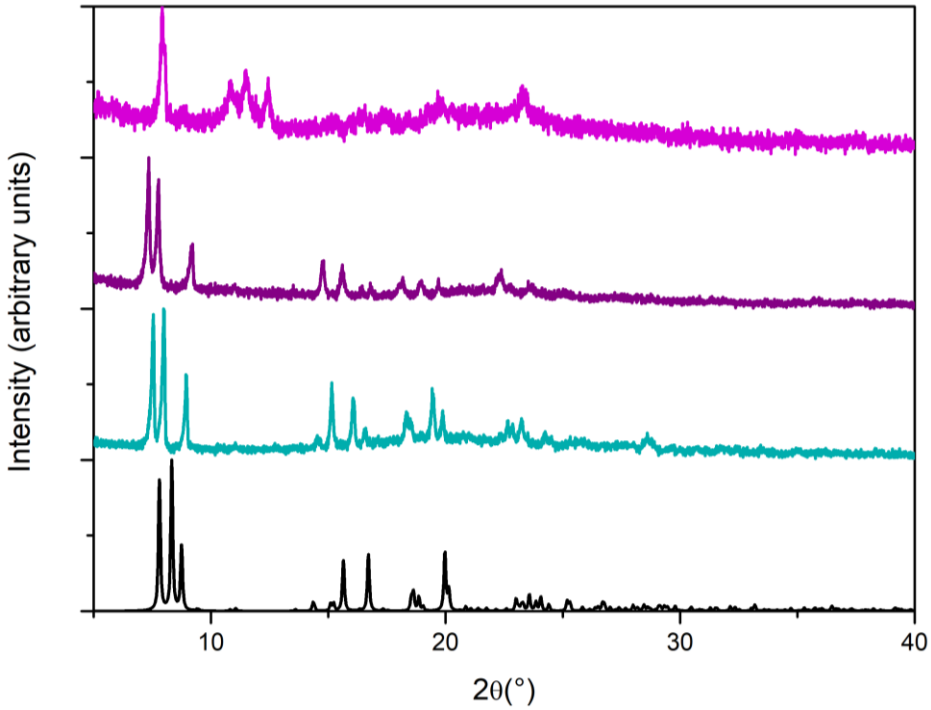

Figure S12. Experimental PXRD plots for MnMOF-L5 as made in DMF (teal), MnMOF-L5 in ethanol (purple), and MnMOF-L5 after adsorption (pink) plotted against simulated MnMOF-L5 (black). Like other flexible MOFs formed with these hinged links, the structure of dried MnMOF-L5 differs slightly from the solvated/as-synthesised material as the wine rack like structures change upon desolvation.

S4. Fourier Transform Infrared (FTIR) Spectra

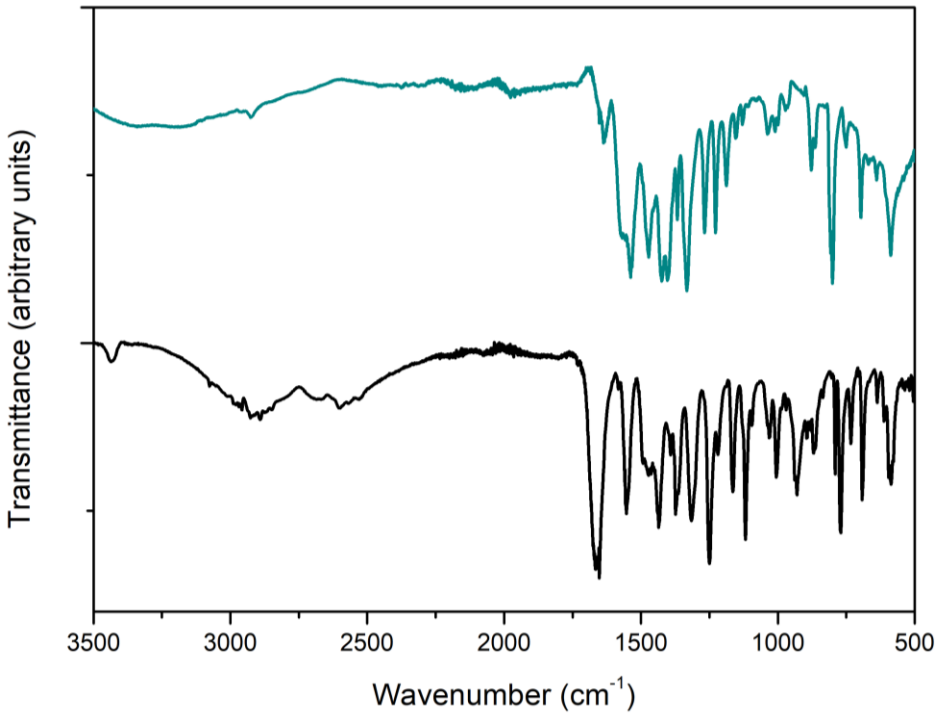

Figure S13. FTIR spectra of H_2**L1**^{Me} (black) and MnMOF-L1^{Me} as made (teal)

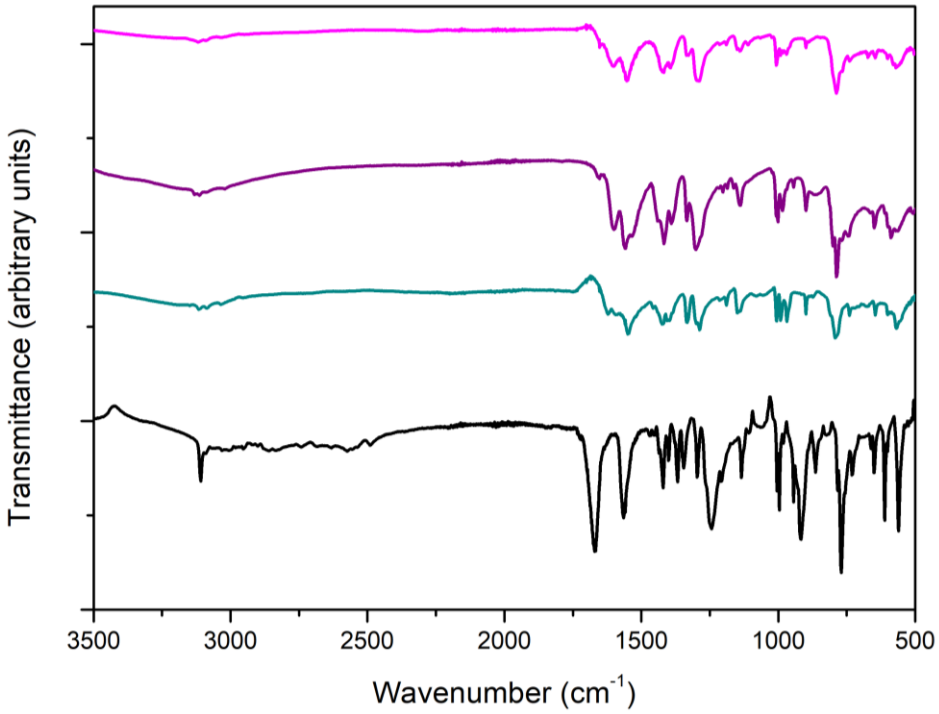

Figure S14. FTIR spectra of H_2**L1** (black), MnMOF-L1-1 as made (teal), MnMOF-L1-2 as made (purple), and MnMOF-L1-3 as made (pink).

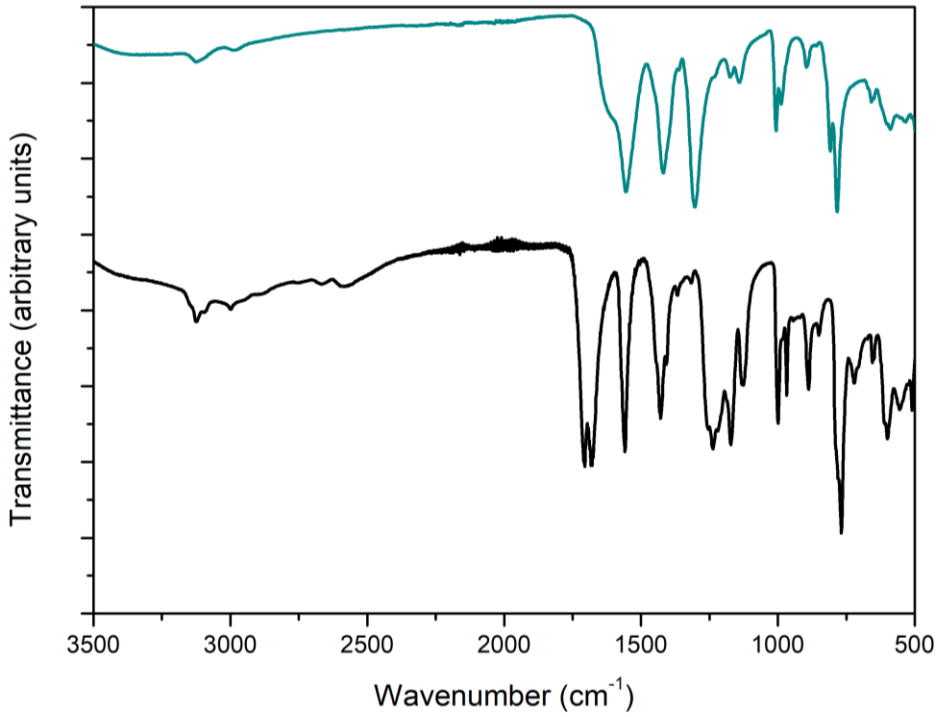

Figure S15. FTIR spectra of H_2**L4** (black), and MnMOF-L4 as made (teal).

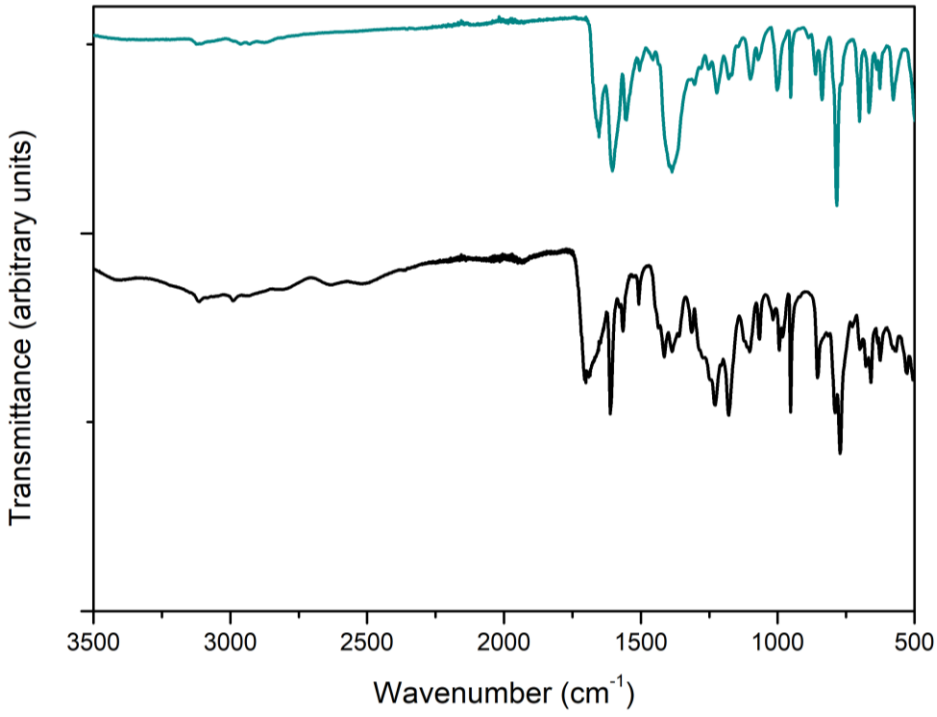

Figure S16. FTIR spectra of H_2**L5** (black), and MnMOF-L5 as made (teal).

S5. Adsorption Data

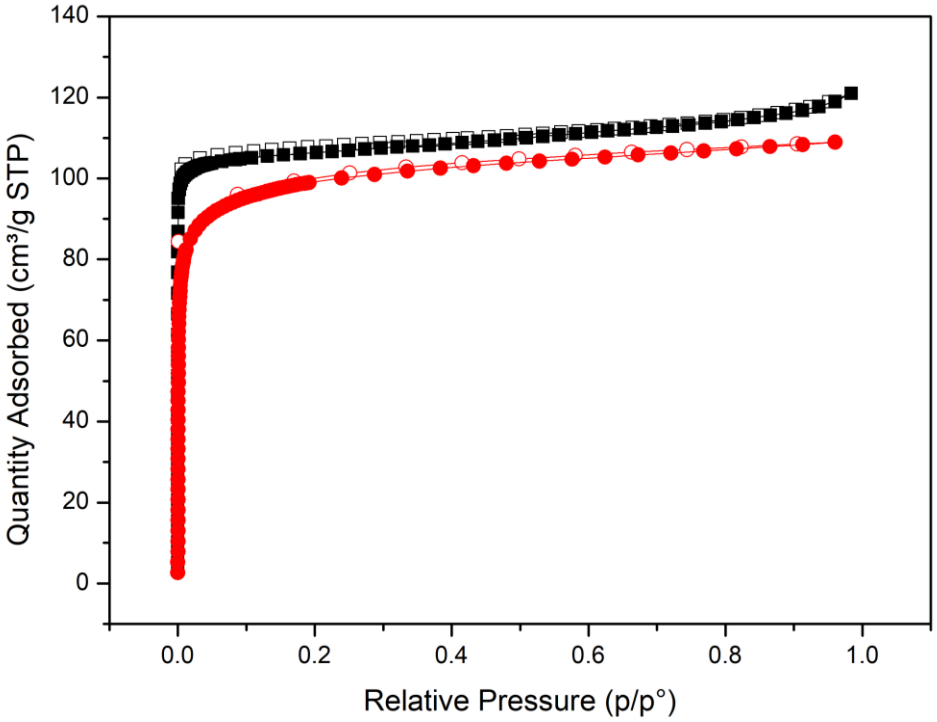

Figure S17. Adsorption data for MnMOF-L4 after activation from dry ethanol at 120°C for 3 h. N_2 at 77 K (black squares) and CO_2 at 195 K (red circles) isotherms. Coloured symbols represent adsorption, open symbols represent desorption. Both isotherms display type 1 behaviour.

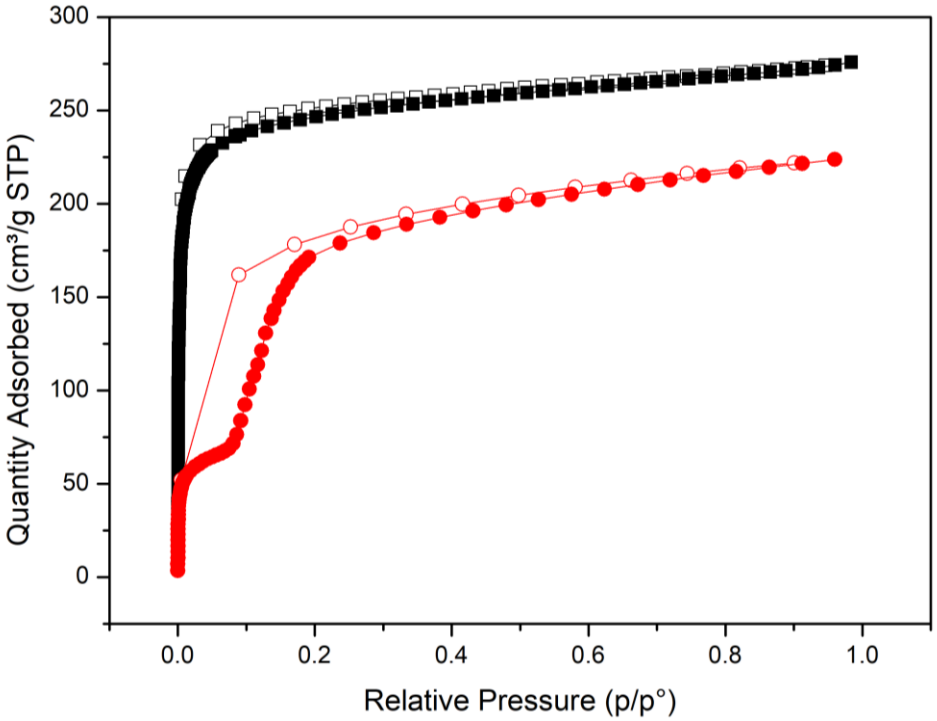

Figure S18. Adsorption data for MnMOF-L5 after activation from dry ethanol at 120°C for 3 h. N_2 at 77 K (black squares) and CO_2 at 195 K (red circles) isotherms. Coloured symbols represent adsorption, open symbols represent desorption. The N_2 isotherm shows type 1 behaviour. The CO_2 isotherm features a step, indicating gate-opening behaviour typical of flexible frameworks.

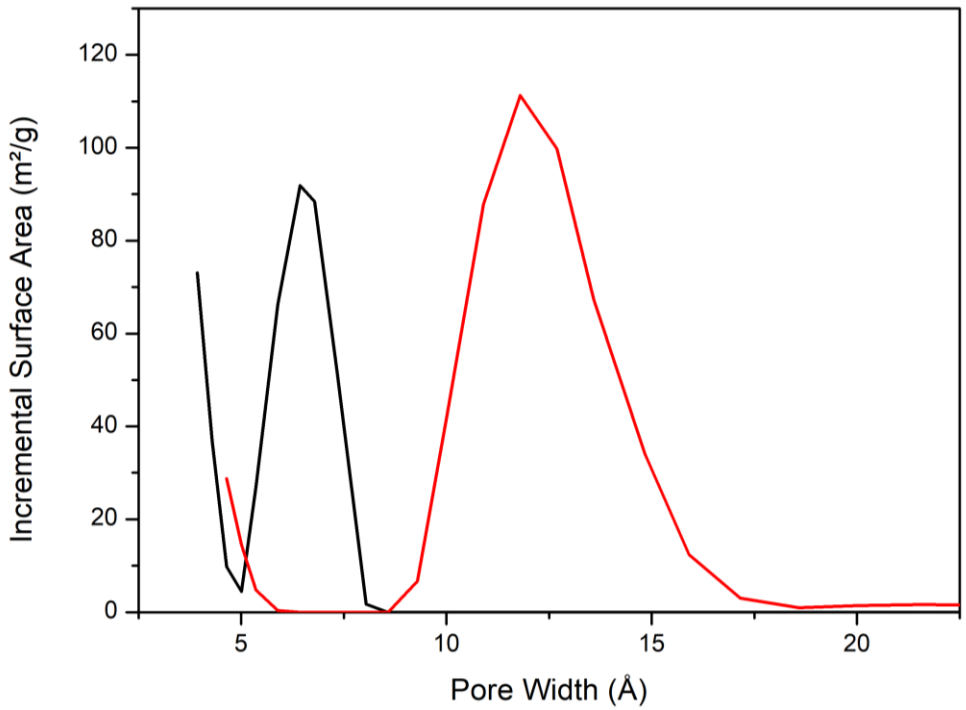

Figure S19 Pore size distribution calculated from the 77 K N_2 adsorption isotherms for **MnMOF-L4** (black) and **MnMOF-L5** (red).

S6. Thermogravimetric Analysis Data

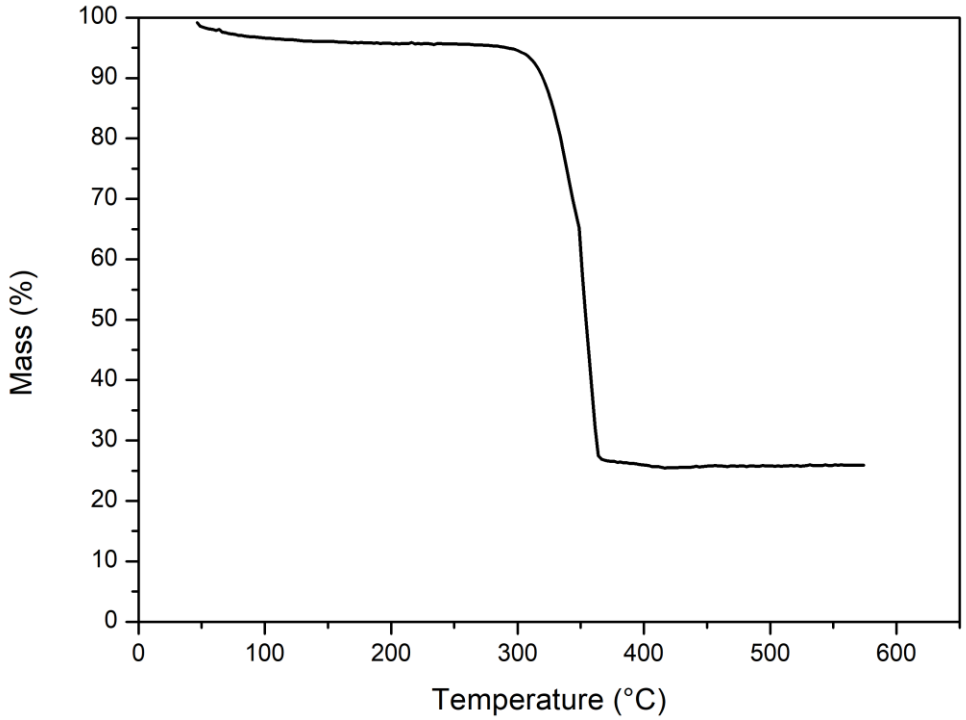

Figure S20. Thermogravimetric analysis of **MnMOF-L4** post-adsorption. Conditions: 45°C – 700°C at 5K/min. The material shows minimal mass loss at low temperatures, indicating that it had been fully activated with no solvent trapped in the pores. MnMOF-L4 decomposed at 350°C.

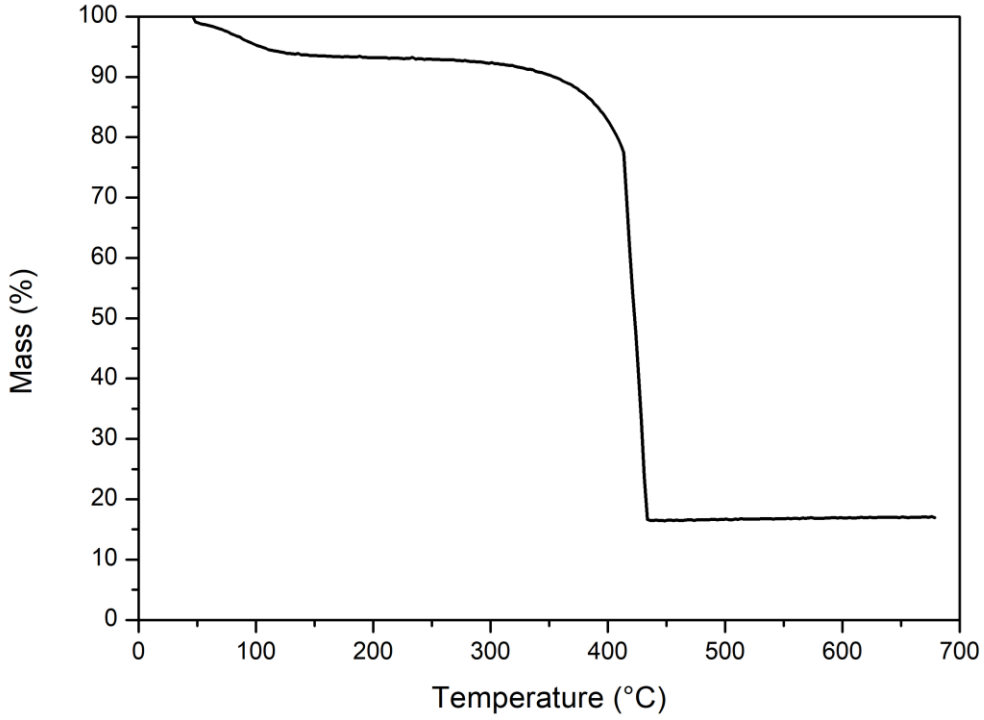

Figure S21. Thermogravimetric analysis of **MnMOF-L5** post-adsorption. Conditions: 45°C – 700°C at 5K/min. The material shows low mass loss at low temperatures, indicating that it had been activated in the adsorption experiment. MnMOF-L5 is thermally stable until it decomposes at 420°C.

S7. Supporting images

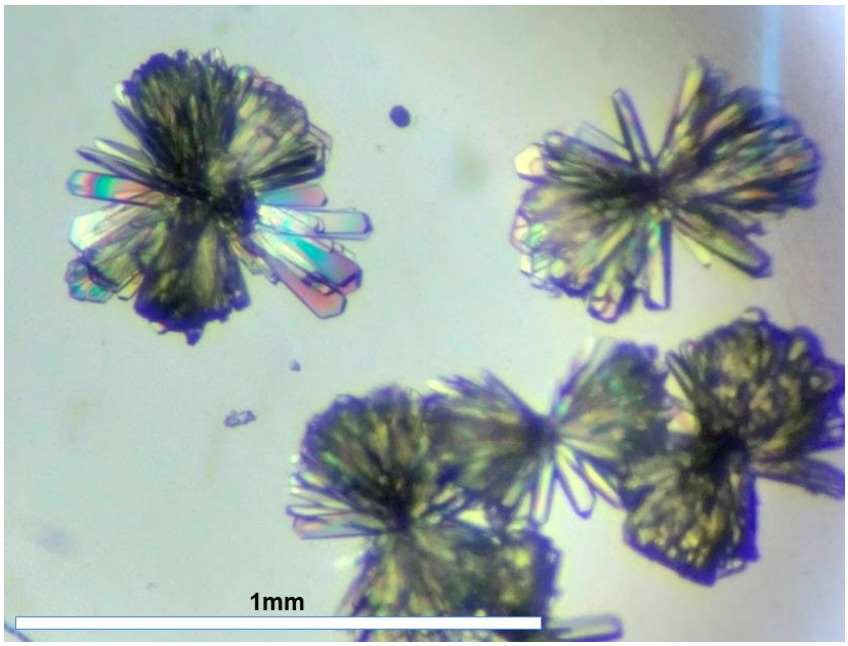

Figure S22. Optical microscope image of clumps of plate-shaped single crystals of MnMOF-L5.

S8. Single crystal X-ray Diffraction (SCXRD)

S8.1. Specific Data and Refinement Details

MnMOF-2D. A SADI restraint was used for the refinement of the coordinated water molecule.

MnMOF-L2. DFIX and DANG restraints were used for the refinement of the coordinated water molecule.

MnMOF-L1-1. Crystals of the major phase were very small and weakly diffracting. Considerable effort was expended to find the "best" crystal and to collect an adequate data set (due to the weak diffraction the completeness to 2theta = 50° was only 91.7%). There was also considerable difficulty in determining the correct space group. Attempts we made to solve the structure in a number of space groups, including the expected monoclinic C-centred space group *C*2/*c*. Despite this being the most likely choice, a chemically sensible solution and refinement could not be achieved. The most chemically reasonable solution was able to be obtained in the monoclinic C-centred space group *Cc*.

Due to the disorder, noted above in the structure description (two distinct networks in a 0.66:0.34 ratio), a large number of restraints were required to give a chemically sensible refinement (EADP, SIMU, RIGU, ISOR restraints).

MnMOF-L1-2. DFIX and DANG restraints were used for the refinement of the coordinated water molecules.

MnMOF-L1-3. One of the linker molecules is partially disordered over two sites. A DMF molecule is disordered over the mirror plane; SIMU and RIGU restraints were required, along with the use of a FREE command to allow the inclusion of hydrogen atoms. A DFIX restraint was used for the refinement of a coordinated water molecule.

MnMOF-L4. DFIX, SIMU, RIGU, ISOR and FLAT restraints were used to allow a chemically sensible refinement of the coordinated and non-coordinated solvent molecules in the structure. The use of a FREE command was required to allow the inclusion of hydrogen atoms on the non-coordinated DMF.

MnMOF-L5. SIMU and RIGU restraints were used to allow a chemically sensible refinement of the non-coordinated DMF molecules.

S8.2. Thermal ellipsoid plots for all structures at the 50% probability level

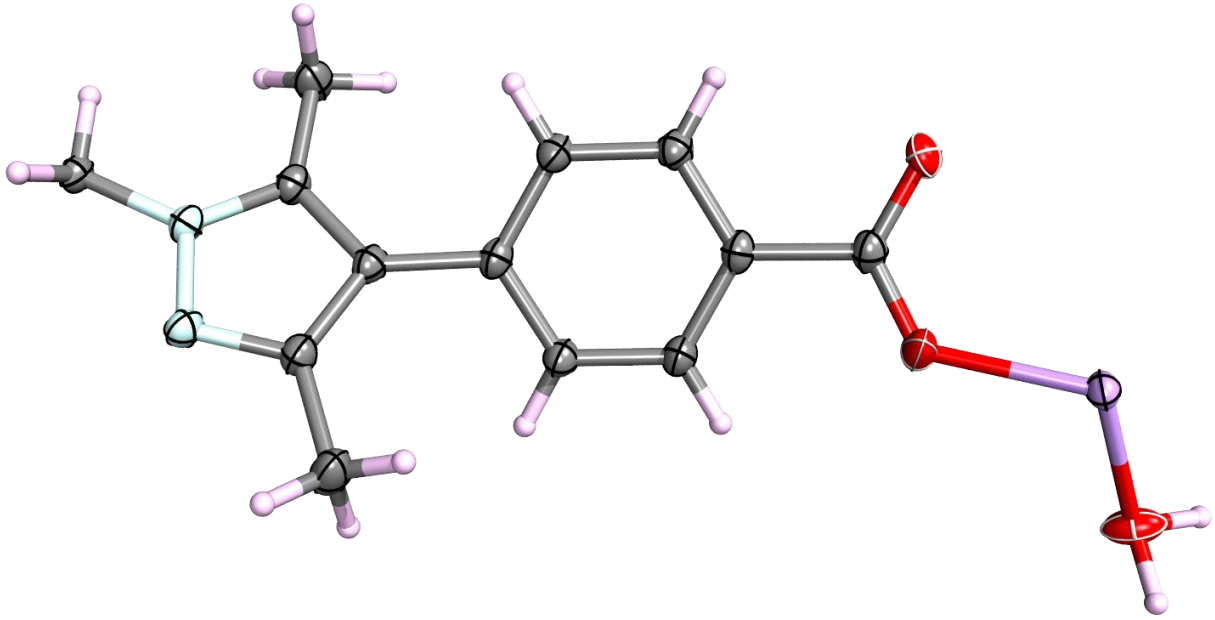

Figure S23. Asymmetric unit of MnMOF-2D, with all non-hydrogen atoms represented by ellipsoids at the 50% probability level (C, grey; H, pink; N, light blue; O, red; Mn, light purple). The ligand is disordered over two positions.

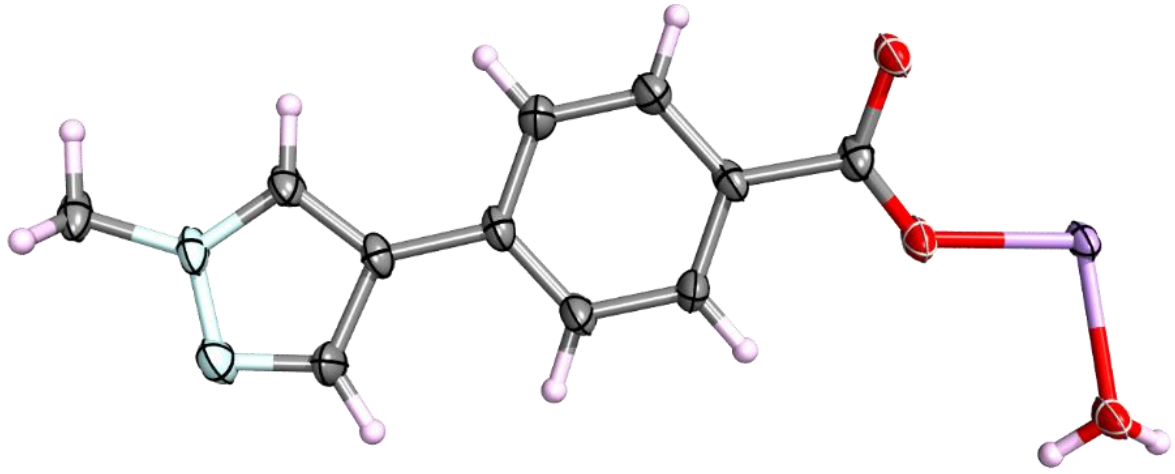

Figure S24. Asymmetric unit of MnMOF-L2, with all non-hydrogen atoms represented by ellipsoids at the 50% probability level (C, grey; H, pink; N, light blue; O, red; Mn, light purple). The ligand is disordered over two positions.

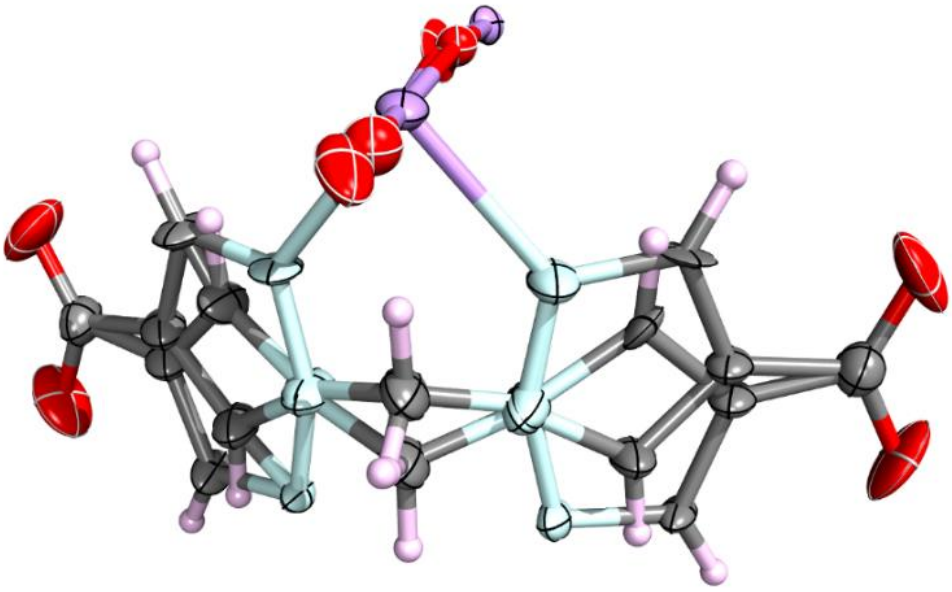

Figure S25. Asymmetric unit of MnMOF-L1-1, with all non-hydrogen atoms represented by ellipsoids at the 50% probability level (C, grey; H, pink; N, light blue; O, red; Mn, light purple). The ligand is disordered over two positions.

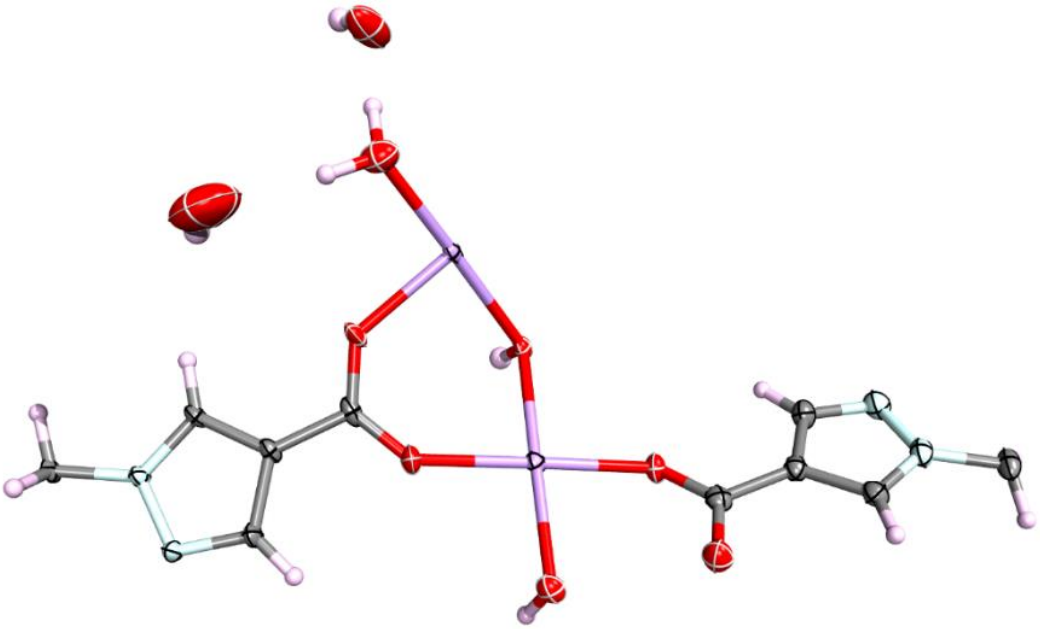

Figure S26. Asymmetric unit of MnMOF-L1-2, with all non-hydrogen atoms represented by ellipsoids at the 50% probability level (C, grey; H, pink; N, light blue; O, red; Mn, light purple).

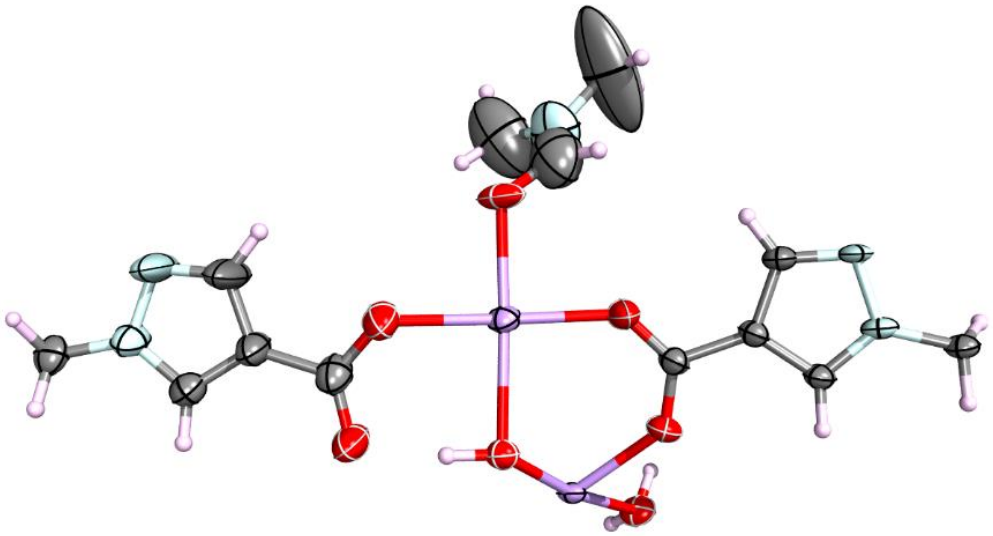

Figure S27. Asymmetric unit of MnMOF-L1-3, with all non-hydrogen atoms represented by ellipsoids at the 50% probability level (C, grey; H, pink; N, light blue; O, red; Mn, light purple).

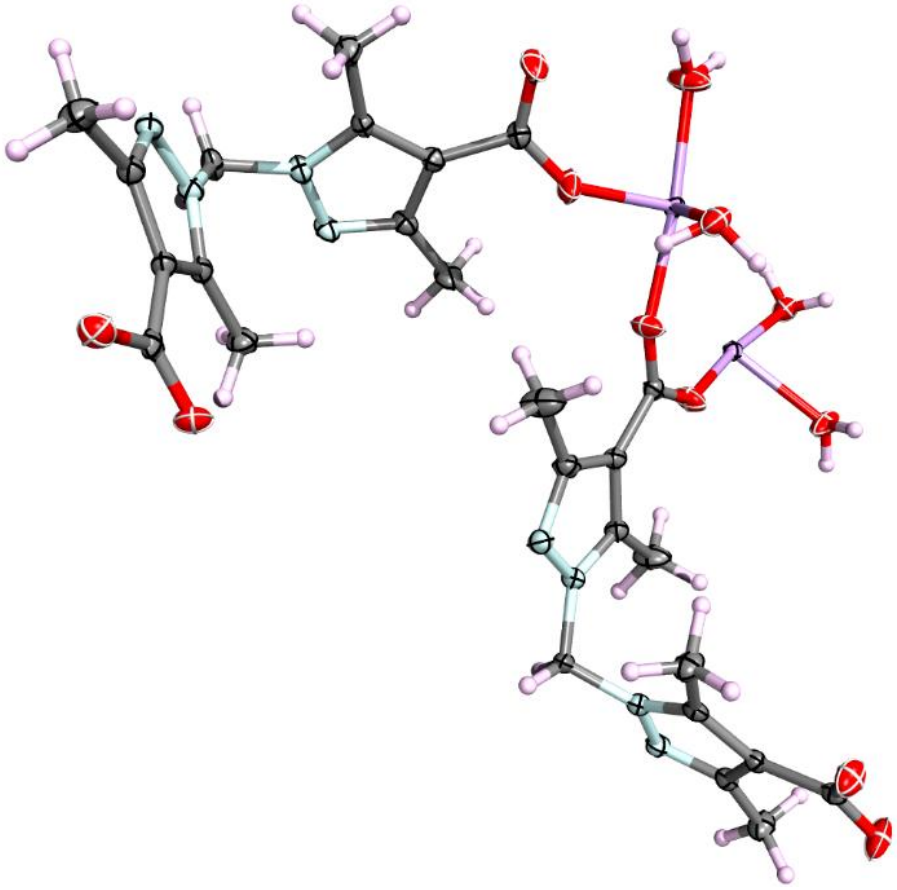

Figure S28. Asymmetric unit of MnMOF-L1^{Me}, with all non-hydrogen atoms represented by ellipsoids at the 50% probability level (C, grey; H, pink; N, light blue; O, red; Mn, light purple).

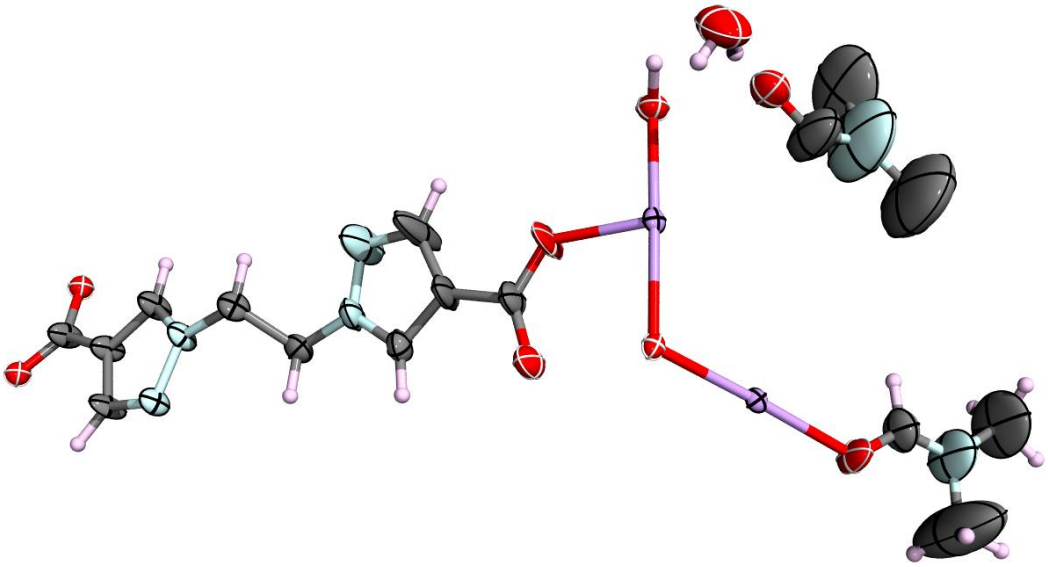

Figure S29. Asymmetric unit of MnMOF-L4, with all non-hydrogen atoms represented by ellipsoids at the 50% probability level (C, grey; H, pink; N, light blue; O, red; Mn, light purple). Hydrogen atoms from a DMF solvate are excluded.

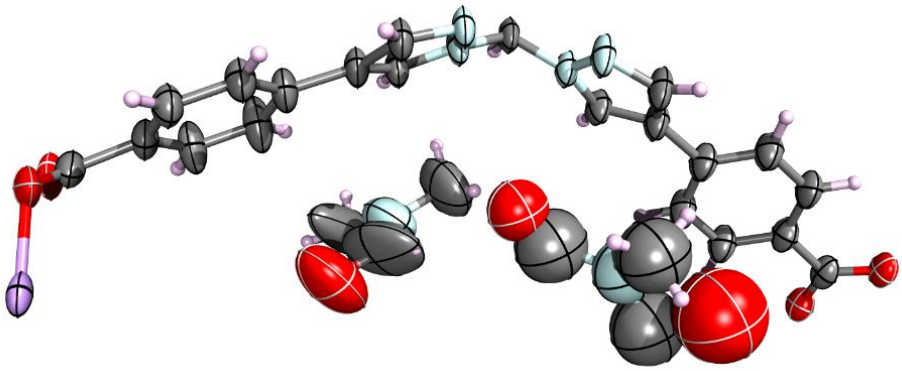

Figure S30. Asymmetric unit of MnMOF-L5, with all non-hydrogen atoms, except a disordered DMF solvate, represented by ellipsoids at the 50% probability level (C, grey; H, pink; N, light blue; O, red; Mn, light purple).

S8.3. Tables of X-ray crystallography data collection and refinement parameters

Table S1.1. Crystallographic data collection and refinement parameters for **MnMOF-2D**, **MnMOF-L2**, **MnMOF-L1-1** and **MnMOF-L1-2**.

Sample	MnMOF-2D	MnMOF-L2	MnMOF-L1-1	MnMOF-L1-2
Crystallographic Parameter				
Formula	$C_{25}H_{24}MnN_4O_5$	$C_{10.5}H_9Mn_{0.5}N_2O_3$	$C_9H_{10}MnN_4O_6$	$C_9H_{11}MnN_4O_{6.5}$
FW	515.42	238.67	325.15	334.16
T, K	300(2)	100(2)	100(2)	150(2)
Wavelength, Å	Mo Kα (λ = 0.71073)	Cu Kα (λ = 1.54184)	Synchrotron (λ = 0.71073)	Mo Kα (λ = 0.71073)
Crystal system, space group	monoclinic, *C2/c*	monoclinic, *I2/a*	Monoclinic, *Cc*	orthorhombic, *Pnnm*
Z	4	8	4	8
a/Å	20.8278(3)	20.3665(10)	14.414(3)	11.4647(4)
b/Å	14.7244(3)	4.5514(2)	10.480(2)	15.9470(6)
c/Å	7.7390(2)	21.1136(9)	7.7400(15)	13.4871(3)
α/°	90	90	90	90
β/°	93.831(2)	101.761(5)	105.64(3)	90
γ/°	90	90	90	90
V/Å^3	2368.07(9)	1916.06(15)	1125.9(4)	2465.81(14)
ρ_{calc}g/cm^3	1.446	1.655	1.918	1.8
Absorption coefficient, mm^{-1}	0.602	6.057	1.209	1.11
F(000)	1068	964	660	1360
Crystal size, mm^3	0.233 × 0.207 × 0.143	0.20 × 0.08 × 0.02	0.1 × 0.07 × 0.03	0.3 × 0.15 × 0.1
2θ range for data collection/°	6.782 to 58.826	8.556 to 152.592	4.87 to 57.082	6.92 to 58.37
Index ranges	-28 ≤ h ≤ 28, -19 ≤ k ≤ 20, -10 ≤ l ≤ 10	-24 ≤ h ≤ 25, -5 ≤ k ≤ 4, -26 ≤ l ≤ 25	-16 ≤ h ≤ 16, -12 ≤ k ≤ 12, -8 ≤ l ≤ 8	-13 ≤ h ≤ 15, -20 ≤ k ≤ 21, -17 ≤ l ≤ 18
Reflections collected	41137	9310	6611	14713
Independent reflections	3106 [R_{int} = 0.0473, R_{sigma} = 0.0287]	1922 [R_{int} = 0.0879, R_{sigma} = 0.0710]	2017 [R_{int} = 0.0377, R_{sigma} = 0.0350]	3154 [R_{int} = 0.0492, R_{sigma} = 0.0448]
Data/restraints/parameters	3106/1/165	1922/4/153	2017/255/238	3154/5/215
GOF on F^2	1.042	1.046	1.033	1.032
Largest diff. peak and hole, eÅ^{-3}	0.28/-0.30	0.40/-0.64	0.41/-0.47	0.99/-0.69
R_1 [I>=2σ (I)]	0.0341	0.0516	0.0645	0.0396
wR_2, all data	0.0875	0.1294	0.1761	0.0860
CCDC Number	2221561	2221562	2221564	2221565

Table S1.2. Crystallographic data collection and refinement parameters for **MnMOF-L1-3**, **MnMOF-L1^{Me}**, **MnMOF-L4** and **MnMOF-L5**.

Sample	MnMOF-L1-3	MnMOF-L1^{Me}	MnMOF-L4	MnMOF-L5
Crystallographic Parameter				
Formula	$C_{21}H_{23}Mn_2N_9O_{11}$	$C_{26}H_{36}N_8O_{12}Mn_2$	$C_{24}H_{29}Mn_2N_{10}O_{13}$	$C_{23.5}H_{18.83}MnN_{4.83}O_{4.83}$
FW	687.36	762.51	775.45	501.22
T, K	293(2)	150(2)	100(2)	100(2)
Wavelength, Å	Mo Kα (λ = 0.71073)	Mo Kα (λ = 0.71073)	Cu Kα (λ = 1.54184)	Cu Kα (λ = 1.54184)
Crystal system, space group	monoclinic, *Cm*	monoclinic, $P2_1/c$	orthorhombic, *Pnma*	monoclinic, *C2/c*
Z	2	4	4	8
a/Å	12.318(3)	9.13640(10)	22.1459(3)	23.2881(7)
b/Å	12.9645(13)	16.5273(3)	12.0673(2)	10.4868(2)
c/Å	9.0482(12)	21.5295(3)	12.5517(2)	24.8587(8)
α/°	90	90	90	90
β/°	107.377(15)	101.7980(10)	90	114.461(4)
γ/°	90	90	90	90
V/Å^3	1379.0(4)	3182.28(8)	3354.33(9)	5526.0(3)
ρ_{calc}g/cm^3	1.655	1.592	1.536	1.205
Absorption coefficient, mm^{-1}	0.991	0.868	6.804	4.247
F(000)	700	1576	1588	2059
Crystal size, mm^3	0.5 × 0.22 × 0.12	0.33 × 0.23 × 0.13	0.087 × 0.069 × 0.066	0.134 × 0.094 × 0.039
2θ range for data collection, °	6.932 to 58.994	6.714 to 58.806	7.984 to 179.28	7.814 to 155.022
Index ranges	-16 ≤ h ≤ 16, -17 ≤ k ≤ 17, -12 ≤ l ≤ 11	-12 ≤ h ≤ 12, -21 ≤ k ≤ 20, -29 ≤ l ≤ 29	-27 ≤ h ≤ 17, -13 ≤ k ≤ 15, -14 ≤ l ≤ 14	-29 ≤ h ≤ 27, -13 ≤ k ≤ 10, -30 ≤ l ≤ 31
Reflections collected	49626	28904	17426	26454
Independent reflections	3616 [R_{int} = 0.0784, R_{sigma} = 0.0332]	7736 [R_{int} = 0.0349, R_{sigma} = 0.0328]	3530 [R_{int} = 0.0319, R_{sigma} = 0.0260]	5632 [R_{int} = 0.0416, R_{sigma} = 0.0267]
Data/restraints/parameters	3616/51/244	7736/7/465	3530/118/260	5632/96/363
GOF on F^2	1.084	1.038	1.191	1.04
Largest diff. peak and hole, eÅ^{-3}	2.31/-0.44	0.64/-0.40	0.91/-1.08	1.11/-0.74
R_1 [I>=2σ (I)]	0.0618	0.0365	0.0876	0.0825
wR_2, all data	0.1673	0.0860	0.2242	0.2577
CCDC Number	2221566	2221563	2221567	2221568

S9. NMR of Digested MOFs Post-adsorption

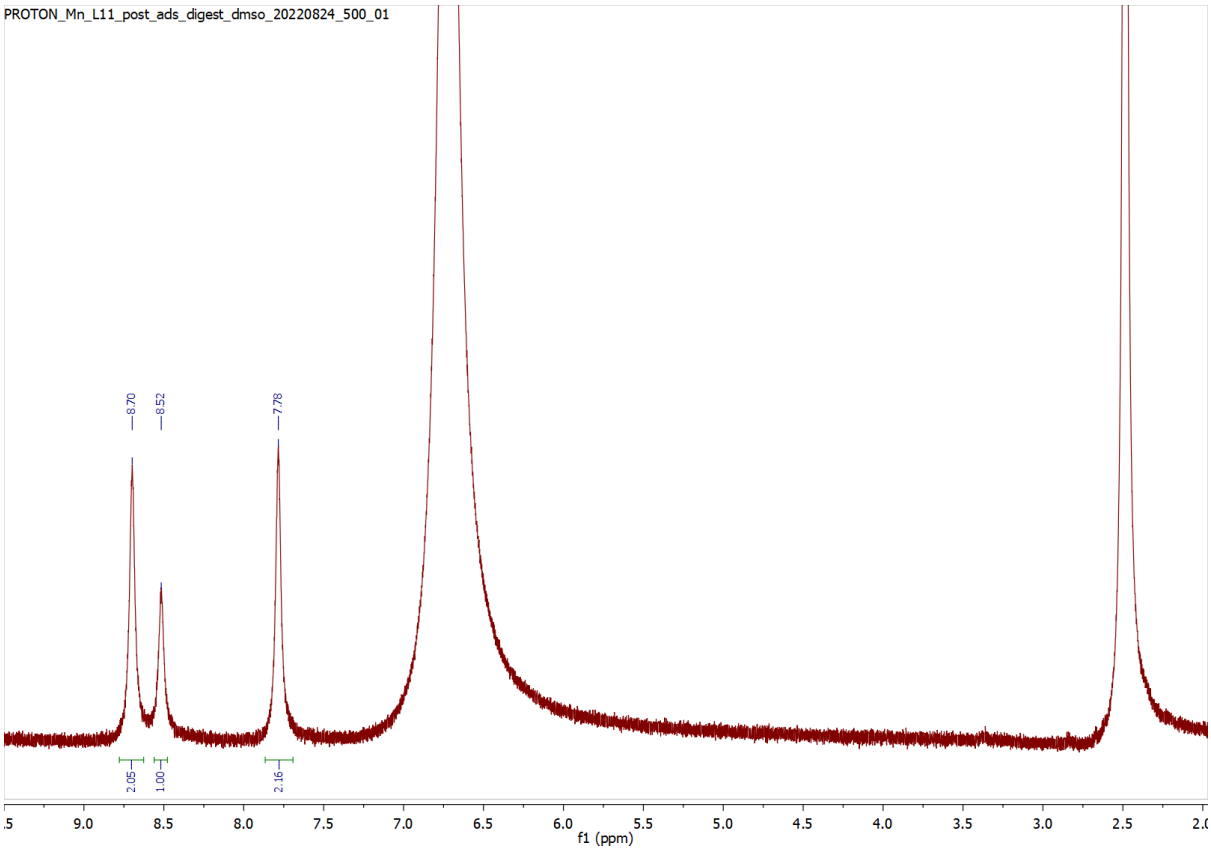

Figure S31. Nuclear magnetic resonance (NMR) data of digested MnMOF-L4 post-adsorption. Digestion conditions: 20 µL conc DCl in 0.5 mL DMSO-d6 at 25°C. The digested MOF shows no peaks indicative of remaining DMF trapped in the pores, indicating full activation. The extra peaks at 2.5 and 6.7 ppm are from DMSO and DCl/D_2O, with the broadness due to Mn(II) in solution.

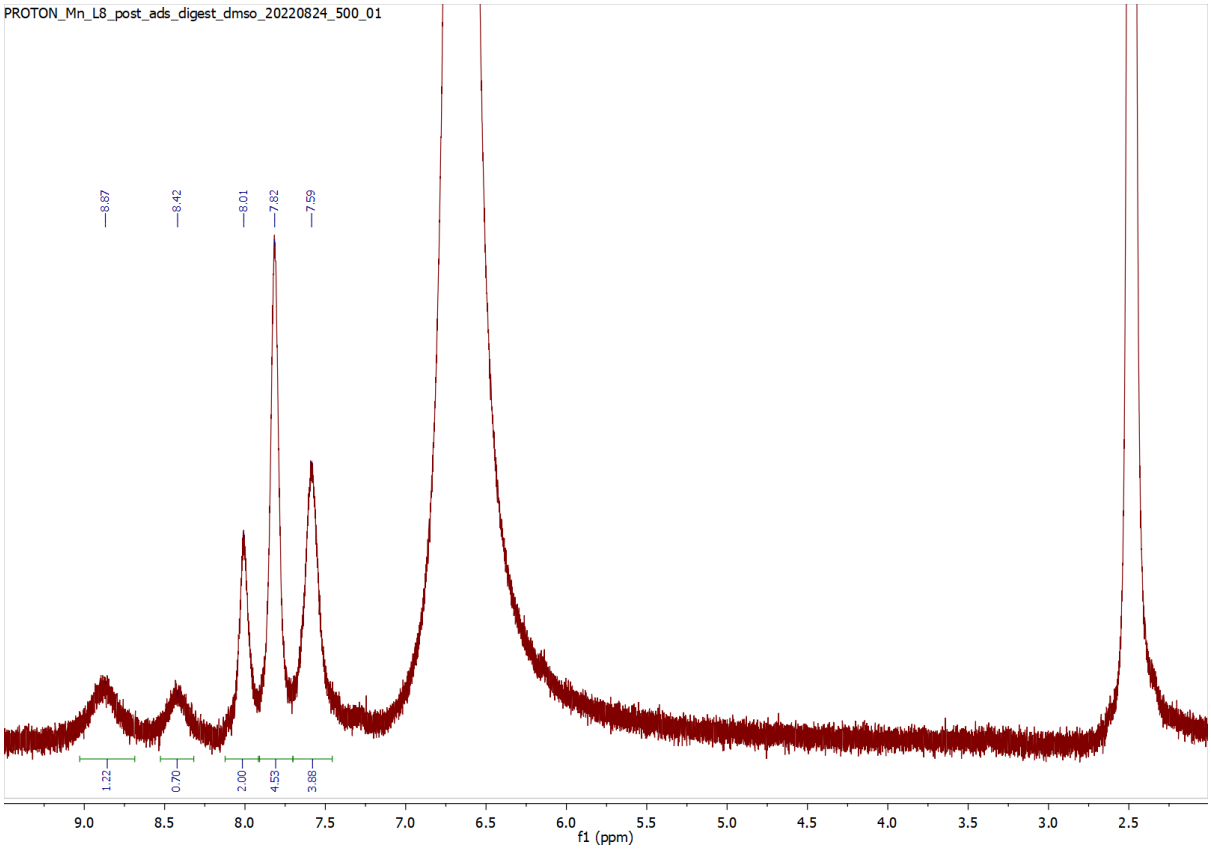

Figure S32. Nuclear magnetic resonance (NMR) data of digested MnMOF-L5 post-adsorption. Digestion conditions: 20 µL conc DCl in 0.5 mL DMSO-d6 at 25°C. The digested MOF shows no peaks indicative of remaining DMF trapped in the pores, indicating full activation. The extra peaks at 2.5 and 6.7 ppm are from DMSO and DCl/D_2O, with the broadness due to Mn(II) in solution.

S10. References

1. H. RimáLim, S. YunáKim, E. HeeáJeon, Y. LanáKim, Y. MiáShin, S. JeanáPark and K. BumáHong, *Chemical Communications*, 2019, **55**, 10424-10427.
2. J.-X. Wang, Z.-R. Zhu, F.-Y. Bai, X.-Y. Wang, X.-X. Zhang and Y.-H. Xing, *Polyhedron*, 2015, **99**, 59-70.
3. W. M. Bloch, R. Babarao, M. R. Hill, C. J. Doonan and C. J. Sumby, *Journal of the American Chemical Society*, 2013, **135**, 10441-10448.
4. W. M. Bloch, C. J. Doonan and C. J. Sumby, *Australian Journal of Chemistry*, 2019, **72**, 797-804.